Acta Biomaterialia 226 (2026) 732–739

Contents lists available at ScienceDirect

Acta Biomaterialia

journal homepage: www.elsevier.com/locate/actbio

Short communication

A calcination-based method for the indirect determination of octacalcium phosphate phase purity

Nicola Döbelin [a,*], Ryo Hamai [b], Kaori Tsuchiya [b], Osamu Suzuki [b,*]

[a] RMS Foundation, Robert Mathys-Strasse 1, Bettlach, 2544, Switzerland
[b] Division of Biomaterials Science Engineering (Division of Craniofacial Function Engineering), Tohoku University Graduate School of Dentistry, Sendai, Japan

ARTICLE INFO

Keywords:
Bioceramics
Bone regeneration
Thermal treatment
Rietveld refinement
Phase quantification
X-ray diffraction

ABSTRACT

Octacalcium phosphate (OCP) is a precursor of bone mineral, but its phase purity is difficult to quantify because of strong peak overlap with biomimetic hydroxyapatite (HAp) in X-ray diffraction (XRD). Here, we present an indirect quantification approach based on the bulk molar Ca/P ratio after controlled calcination. Upon thermal treatment, OCP, HAp, and amorphous calcium phosphate decompose into a binary mixture of β-calcium pyrophosphate (β-CPP) and β-tricalcium phosphate (β-TCP), which can be reliably quantified by XRD. From their relative amounts, the bulk Ca/P ratio and an equivalent OCP phase content can be calculated. Because phosphate evaporation during calcination alters the β-CPP/β-TCP equilibrium and biases the derived Ca/P ratio, we demonstrate that stabilizing the furnace atmosphere is essential for reproducible results. Saturating the atmosphere with sacrificial monetite effectively suppresses phosphate loss and preserves the original composition. By varying dwell time between 2 and 24 h at two temperatures, we delimit the processing window within which the derived phase content is independent of the treatment conditions. At 1000°C, this approach yields stable and reproducible OCP phase contents with negligible compositional drift over dwell times up to 24 h. The method is simple to implement and provides a robust tool for assessing OCP phase purity in both research and quality control settings.

Statement of significance: Octacalcium phosphate (OCP) is an important precursor of bone mineral, yet its phase purity is difficult to quantify due to strong X-ray diffraction peak overlap with biomimetic hydroxyapatite. In this study, we present a simple and reproducible indirect method to assess OCP phase purity based on the bulk Ca/P ratio after controlled calcination and quantitative phase analysis of the resulting high-temperature phases. We demonstrate that phosphate evaporation during calcination can significantly bias the calculated Ca/P ratio and show that stabilizing the furnace atmosphere using sacrificial monetite effectively suppresses this effect. At 1000°C, the method yields stable and reproducible OCP phase purity values over extended dwell times, making it suitable for both research and quality control applications.

1. Introduction

Octacalcium phosphate (OCP, $Ca_8H_2(PO_4)_6{\cdot}5H_2O$) occurs in the early stages of bone mineralization and is regarded as a precursor of natural bone mineral [1,2]. In fact, recent study showed that OCP is involved at the initial bone apatite crystal formation in rat and human bones [3]. As a synthetic bone substitute, however, it has received less attention than hydroxyapatite (HAp, $Ca_5(PO_4)_3OH$) and β-tricalcium phosphate (β-TCP, $Ca_3(PO_4)_2$), despite evidence that OCP supports bone regeneration either alone, in composites, or as a carrier for drugs and ions [4–6]. Recently, efforts to commercialize OCP-based grafts have increased, underlining the need for reliable methods of characterization [7]. However, a robust, reproducible, and readily available method for quantifying the OCP phase purity is still lacking.

The crystal structure of OCP closely resembles that of HAp, consisting of HAp-like layers separated by hydrated layers containing H_2O molecules and HPO_4 groups [8]. During hydrolysis, these hydrated layers are eliminated and the HAp layers merge, forming larger domains of biomimetic HAp [9,10] and strongly reducing the size of coherent OCP domains. In addition to OCP and biomimetic HAp, amorphous calcium phosphate (ACP, $Ca_3(PO_4)_2 \cdot nH_2O$) [11,12] may also be present. Because of the structural similarity and the nanocrystalline nature

* Corresponding authors.
E-mail addresses: nicola.doebelin@rms-foundation.ch (N. Döbelin), suzuki-o@tohoku.ac.jp (O. Suzuki).

https://doi.org/10.1016/j.actbio.2026.10.008
Received 6 February 2026; Accepted 2 October 2026
Available online 3 October 2026
1742-7061/© 2026 The Authors. Published by Elsevier Inc. on behalf of Acta Materialia Inc. This is an open access article under the CC BY-NC-ND license (http://creativecommons.org/licenses/by-nc-nd/4.0/).

of typical samples, the X-ray diffraction (XRD) patterns of OCP and HAp strongly overlap, making direct quantification unreliable. Specifically, the OCP (0 0 2) peak at $d = 3.41361$ Å overlaps with the HAp (0 0 2) peak at $d = 3.439500$ Å [13], and the group of OCP (3 −3 1), OCP (−4 0 2), and OCP (6 0 1) at $d = 2.83769$, 2.82366, and 2.77567 Å, respectively, overlaps with the characteristic group of HAp (2 1 1), HAp (1 1 2), and HAp (3 0 0) at $d = 2.81468$, 2.77811, and 2.72047 Å. A minor CDHA fraction therefore contributes no independent signal, and its intensity is readily absorbed by the refined profile parameters of the OCP model. This is compounded by three further effects: CDHA formed by OCP hydrolysis is nanocrystalline, so that its reflections are severely broadened and merge with the background; it forms topotactically within the OCP crystals rather than as a discrete second phase, so that the assumptions underlying quantitative phase analysis are only approximately satisfied; and any amorphous fraction remains invisible to XRD altogether. While OCP possesses a diagnostic low-angle reflection at $d = 18.6$ Å (OCP (1 0 0) at 4.738 °2θ for Cu$K\alpha$), it cannot itself serve as a quantitative measure either, as its intensity is strongly affected by the preferred orientation of the plate-like OCP crystals. Furthermore, the low diffraction angle exposes instrumental inaccuracies emerging from an extremely narrow divergence slit opening, which is necessary to avoid beam overflow. Instrumental inaccuracies and beam overflow both result in unreliable intensity of the OCP (1 0 0) reflection, which further reduces its suitability for phase quantification.

The hydrolysis of OCP to hydroxyapatite (HAp) proceeds via calcium-deficient apatite (CDHA, $Ca_{10-x}(HPO_4)_x(PO_4)_{6-x}(OH)_{2-x}$) intermediates. Nelson and McLean demonstrated that the Ca/P ratio of the reaction products increases progressively from ~1.32 (OCP) toward ~1.64 (HAp), with intermediate compositions corresponding to CDHA [14]. Nelson et al. later reported that apatite-like phases formed on OCP seeds under near-physiological conditions could be characterized by a Ca/P ratio of 1.50 ± 0.04, consistent with CDHA of composition $Ca_9(HPO_4)(PO_4)_5OH$ [15]. Our previous study also confirmed by chemical analysis that CDHA produced from OCP hydrolysis typically exhibits a Ca/P ratio of ~1.5 [16]. Based on this evidence, we approximate the Ca/P ratio of CDHA in partially hydrolyzed OCP samples as 1.50. With this assumption, the bulk Ca/P ratio of the calcined samples can serve as a proxy to calculate equivalent mixtures of OCP and CDHA to estimate the OCP phase purity prior to thermal treatment.

Here, we propose an indirect approach based on the molar Ca/P ratio of calcined samples as a proxy for determining the OCP phase purity. The method specifically targets the quantification of CDHA formed by OCP hydrolysis during or after the synthesis.

Because the approach relies on a thermal treatment step, its validity depends on the existence of a processing window in which the measured Ca/P ratio faithfully reflects the composition of the untreated sample. This window is delimited by two competing constraints: at short dwell times, decomposition and recrystallization into the binary β-CPP/β-TCP assemblage may be incomplete, whereas at long dwell times, evaporation of phosphorus species progressively converts β-CPP into β-TCP and biases the derived Ca/P ratio. Effective suppression of phosphorous evaporation by addition of sacrificial monetite ($CaHPO_4$) to create a phosphorous-saturated atmosphere was previously demonstrated by Döbelin et al. [17]. The aim of this study was therefore to delimit this window and to demonstrate that the derived OCP phase content is insensitive to the thermal treatment conditions within it. Dwell time, temperature, and furnace atmosphere were varied as validation parameters rather than as process parameters to be optimized.

2. Materials and methods

For wet synthesis of OCP, calcium acetate monohydrate (FUJIFILM Wako Pure Chemical Co., Osaka, Japan; ≥ 99.0%) and sodium dihydrogen phosphate dihydrate (FUJIFILM Wako Pure Chemical Co.; ≥ 99.0%) were selected as the source reagents. OCP was synthesized through the direct precipitation method based on the previous literature [18,19]. Briefly, the calcium acetate solution and sodium dihydrogen phosphate solution were slowly mixed in an equal molar ratio with stirring at 100 rpm under controlled pH (< 5.5, monitored by a pH meter under corresponding temperature) at 65°C. The final volume of the reacting solution was 2 L, and the final concentration of the source reagent was 0.08 M. OCP precipitated from the solution following equation (1):

$$8(CH_3COO)_2Ca + 6NaH_2PO_4 + 5H_2O \rightarrow Ca_8H_2(PO_4)_6 \cdot 5H_2O + 6CH_3COONa + 10CH_3COOH \quad (1)$$

The pH in the reacting solution was buffered according to equation (1). The precipitate was separated by filtering and washed with ultrapure water several times at room temperature. The washed precipitate was dried for 24 h at 105°C. The dried cake was crushed manually and passed through a 500 μm testing sieve for subsequent calcination and XRD measurement.

The synthesized OCP was analyzed by X-ray diffraction (Miniflex 600, Rigaku Co., Tokyo, Japan), Fourier transform infrared spectroscopy (FT-IR; FT/IR-4600, JASCO Co., Tokyo, Japan), and 400 MHz solid-state nuclear magnetic resonance (NMR; ECZL-400, JEOL Ltd., Tokyo, Japan). The XRD pattern of the synthesized OCP was acquired using monochromatized CuKα (40 kV and 15 mA) from 2θ = 3° to 60° at a scanning rate of 3.0°/min, with diffraction detection at 0.02° step intervals. The FT-IR spectrum of OCP mixed with KBr was measured in the range of 1400–400 cm^{-1} with a resolution of 4 cm^{-1}. The ^{31}P magic angle spinning (MAS) NMR spectrum of OCP was acquired at a MAS frequency of 15 kHz with ^{1}H decoupling at 100 kHz during acquisition. The ^{31}P chemical shifts were externally referenced to 85% H_3PO_4 at 0 ppm.

The method for quantification of the molar Ca/P ratio of OCP samples was inspired by ISO 13779–3 [20]. Briefly, this method subjects calcium phosphate samples to a thermal treatment at 1000°C for 15 h, which induces recrystallization and phase decomposition, resulting in a binary system of highly crystalline phases of stoichiometric composition. The phases are then quantified by XRD, and the bulk Ca/P ratio is calculated from the phase quantities. We adapted the approach of converting the initial phase composition into a simple, highly crystalline phase assembly by thermal treatment from ISO 13779–3 to the OCP–CDHA system (Ca/P ≈ 1.33–1.50). To delimit the processing window within which the derived Ca/P ratio is independent of the thermal treatment conditions, calcination series were conducted at 1000°C and 1100°C for dwell times of 2, 4, 8, 16, and 24 h, with and without saturating the furnace atmosphere with phosphorus species. The dwell times were chosen to span the 15 h specified in ISO 13779–3 and to extend to substantially shorter times, so that both incomplete conversion at the lower end and phosphate loss at the upper end would become detectable. To achieve saturation, ~2 g of sacrificial monetite (DCPA, $CaHPO_4$) was placed around three crucibles containing ~0.2 g of OCP each. Monetite converts to γ-CPP (γ-$Ca_2P_2O_7$) between 270 and 430°C, and to β-CPP (β-$Ca_2P_2O_7$) between 750 and 850°C [21]. The β-CPP phase was reported to create a phosphate-saturated atmosphere that is in a thermodynamic equilibrium with the OCP decomposition phases β-CPP and β-TCP [17], which provided the rationale for selecting monetite as the sacrificial source of volatile phosphorous species in this study. The setup was covered with an inverted Al_2O_3 crucible to minimize the gas volume over the samples (Fig. 1). The assembly was introduced into a cold furnace (CDF 15/1B, Carbolite, Hope Valley, England), heated to the target temperature, held for the programmed dwell time, and then cooled at maximum rate. The target temperature of 1000°C was reached after 26 min, and 1100°C after 35 min. Cooling to 300°C took approximately 3 h in both cases. The samples were retrieved from the furnace once the temperature had reached the range of 300 to 100°C, which was low enough for the base plate and the crucibles to tolerate the thermal shock when being taken out of the furnace and placed on a ceramic plate without cracking. For two selected conditions



Fig. 1. Experimental setup for the calcinations. Left: Samples calcined in open atmosphere. Center: Sacrificial monetite was placed around the samples. Right: The samples and sacrificial monetite were covered with another crucible to minimize the gas volume over the samples during the calcination in saturated atmosphere.

(1000°C for 2 h in saturated atmosphere, and 1100°C for 24 h in open atmosphere), the calcination was repeated with the crucibles weighed before and after the thermal treatment on an analytical balance (Mettler Toledo, ± 0.00002 g) in order to determine the mass loss gravimetrically. These measurements served as an independent consistency check and were not used in the determination of the Ca/P ratio.

The calcined powders were milled by hand in ethanol using an agate mortar and then transferred as a suspension onto a microscopy cover slide in an XRD sample holder and left to dry. Ethanol evaporated more rapidly than isopropanol and water, which thus reduced the risk for crystal alignment during the drying process. XRD data were collected on a Bruker D8 diffractometer (Bruker AXS SE, Karlsruhe, Germany) from 5 to 80 °2θ and analyzed by Rietveld refinement using the software Profex [22]. Since XRD data was collected after the heat treatment converting OCP and CDHA to a mixture of β-CPP and β-TCP, it was not necessary to acquire XRD data below 5 °2θ (using CuKα radiation) to capture the OCP (1 0 0) peak at 4.738 °2θ. Neither β-CPP nor β-TCP contain peaks below 10 °2θ. Structural models were taken from Dickens et al. [23] for β-TCP, and from Boudin et al. [24] for β-CPP. Peak intensities I_0 were modulated with a 2θ dependent correction factor according to Eq. (2) to account for transparency of the thin suspension layer on the microscopy slides:

$$I = I_0 \cdot \left(1 - \exp\left(-\frac{s}{\sin(\theta)}\right)\right) \tag{2}$$

s was a refined factor representing the product of the sample absorption factor μ and layer thickness d. The Ca/P ratio (CaP) and equivalent OCP phase quantity (OCP_{eq}) were derived from the refined β-CPP and β-TCP contents ($Q_{\beta\text{-}TCP}$ and $Q_{\beta\text{-}CPP}$) using molecular weights of $M_{\beta\text{-TCP}}$ = 310.1767 g/mol, $M_{\beta\text{-CPP}}$ = 254.0993 g/mol, M_{OCP} = 982.4598 g/mol, and M_{CDHA} = 948.5454 g/mol according to Eqs. (3) and (4):

$$CaP = \frac{3 \cdot \frac{Q_{\beta-TCP}}{M_{\beta-TCP}} + 2 \cdot \frac{Q_{\beta-CPP}}{M_{\beta-CPP}}}{2 \cdot \frac{Q_{\beta-TCP}}{M_{\beta-TCP}} + 2 \cdot \frac{Q_{\beta-CPP}}{M_{\beta-CPP}}} \tag{3}$$

$$OCP_{eq} = 100 \cdot \frac{6 \cdot CaP \cdot M_{OCP} - 9 \cdot M_{OCP}}{8 \cdot M_{CDHA} + 6 \cdot CaP \cdot (M_{OCP} - M_{CDHA}) - 9 \cdot M_{OCP}} \tag{4}$$

Mean values and standard deviations were calculated from triplicate measurements.

Statistical analysis. All experiments were performed in independent triplicate (n = 3), with three separately prepared OCP aliquots taken from the same synthesis batch, calcined and analyzed by XRD/Rietveld refinement for each combination of temperature (1000°C, 1100°C), atmosphere (saturated with sacrificial monetite, or unsaturated), and dwell time (2, 4, 8, 16, 24 h), giving 60 independent measurements in total. Data are reported as mean ± standard deviation. For each of the four temperature × atmosphere conditions, the dependence of the equivalent OCP content (OCP_{eq}) on dwell time was assessed by linear regression; slopes are reported with their 95% confidence intervals, and a slope significantly different from zero ($p < 0.05$) was taken as evidence of compositional drift over the investigated dwell-time window. Differences in reproducibility between the four conditions were evaluated by Levene's test (Brown–Forsythe variant, median-centered) on the within-time-point residuals of OCP_{eq}. The combined effects of temperature, atmosphere, and their interaction on OCP_{eq} were assessed by two-way ANOVA pooled over dwell times (n = 15 per condition), followed by Tukey's HSD post-hoc test for pairwise comparison of the four conditions. Because the sample size per individual time-point cell (n = 3) was too small for meaningful formal normality testing, results are interpreted with this limitation in mind; the conclusions are however supported by the consistent picture obtained from regression, variance, and ANOVA-based approaches. The significance threshold was set at $\alpha = 0.05$ throughout. Calculations were performed in Origin 2026 (OriginLab Corporation, Northampton, MA, USA) and cross-verified in Microsoft Excel using LINEST and standard array formulas.

3. Results

Fig. 2 shows the XRD pattern, FT-IR spectrum, and ^{31}P MAS NMR spectrum of the synthesized OCP. In the XRD pattern (Fig. 2A), the typical diffraction peaks corresponding to (1 0 0), (0 1 0), (0 0 2), (−5 3 0), and (7 0 0) in the OCP lattice were detected at 2θ = 4.7, 9.8, 25.9, 31.8, and 33.6°, respectively (PDF# 00–079–0423, International Centre for Diffraction Data, ICDD). No diffraction signals of other calcium phosphates, such as HAp and DCPD ($CaHPO_4 \cdot 2H_2O$), were observed in the XRD pattern. In the FT-IR spectrum (Fig. 2B), the infrared absorption bands attributed to ν_3 HPO_4(6), ν_3 HPO_4(5), ν_3 PO_4/HPO_4, and ν_3 PO_4 were detected at 1120, 1105, 1075, and 1037 cm^{-1}, respectively [25]. The HPO_4(5) and HPO_4(6) are located in the hydrated layer and at the junction of the CDHA layer and the hydrated layer of the OCP lattice, respectively. Furthermore, the absorption bands corresponding to [P–(OH)] stretch of HPO_4(6) and HPO_4(5) were observed at 910, and 862 cm^{-1}, respectively. In the ^{31}P MAS NMR spectrum (Fig. 2C), the peaks attributed to phosphorus of PO_4^{3-} and HPO_4^{2-} in the OCP lattice were detected at 3.4, 3.1, 1.7, and −0.4 ppm [26,27]. However, no peaks corresponding to HAp [28] and DCPD ($CaHPO_4 \cdot 2H_2O$) [29] were observed in the spectrum. The NMR analysis indicated that the synthesized sample was a single phase of OCP.

The XRD datasets of thermally treated OCP samples showed signals of highly crystalline β-CPP and β-TCP with peak resolution near the instrument's optical limit. The phase signals were well separated and allowed for accurate quantification by Rietveld refinement (Fig. 3).

Table 1 summarizes the quantitative phase analysis of the calcined samples (only β-CPP is reported; β-TCP values can be reconstructed as 100 – β-CPP). Equivalent OCP values (OCP_{eq}) were calculated from the Ca/P ratios.

Fig. 4 represents the calculated OCP_{eq} phase purity as a function of processing temperature, time, and atmospheric condition. At 1100°C without atmosphere saturation, the β-CPP/β-TCP ratio decreased

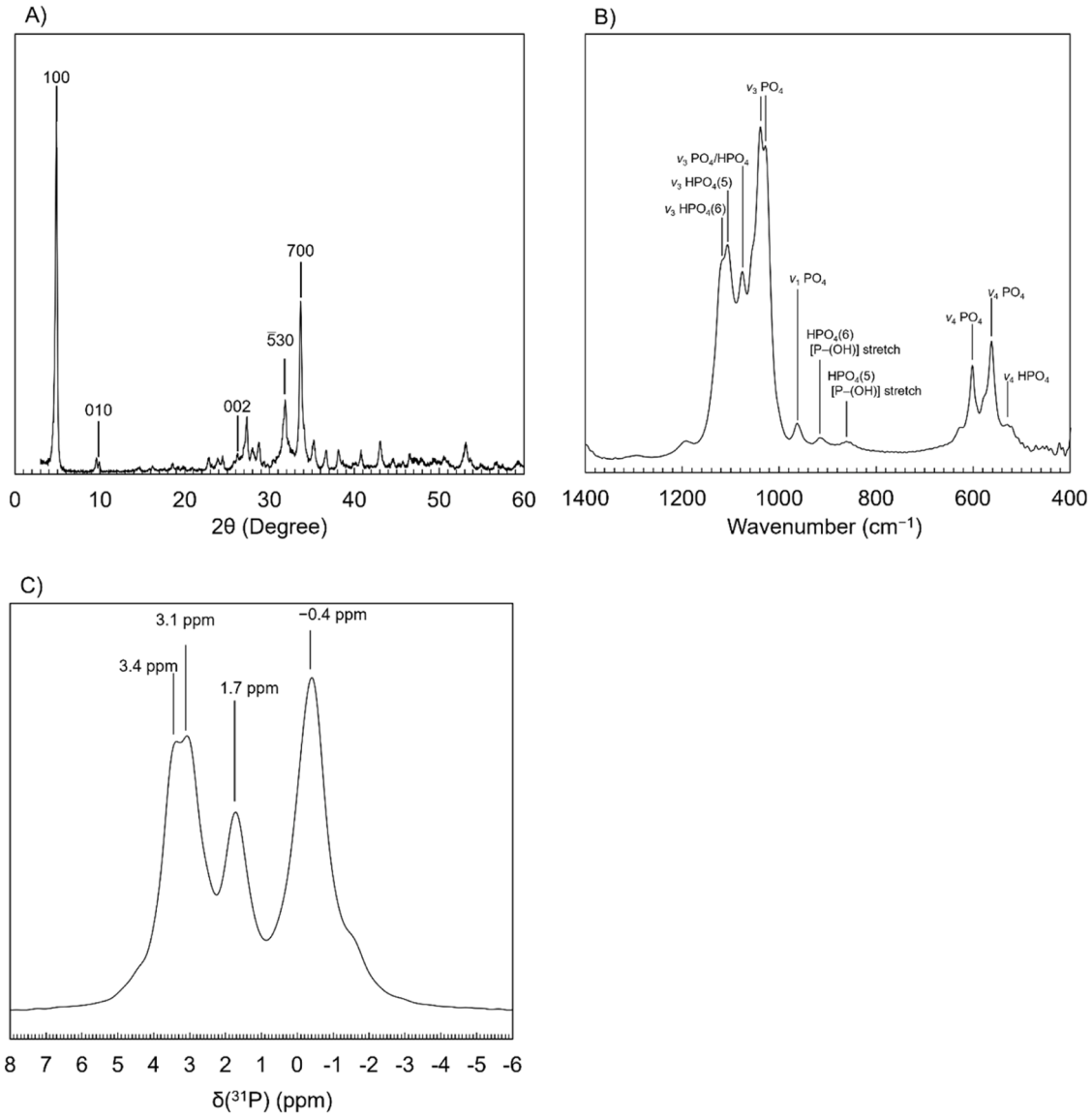

Fig. 2. (A) XRD pattern, (B) FT-IR spectrum, and (C) ^{31}P MAS NMR spectrum of synthesized OCP. The ^{31}P MAS NMR spectrum was measured at a MAS frequency of 15 kHz with ^{1}H decoupling at 100 kHz.

markedly within 16 h due to phosphate evaporation. The bulk Ca/P ratio increased from 1.351 ± 0.001 to 1.410 ± 0.007 (ΔCaP = 0.059). Linear regression of OCP_{eq} versus dwell time confirmed a strong significant downward drift in this condition (slope = –1.67 wt%/h, 95% CI [–2.12, –1.22], $p < 10^{-5}$, $R^2 = 0.83$). This compositional drift led to a discrepancy between the original and current Ca/P ratios, resulting in misinterpretation of OCP purity. Reproducibility was also compromised, as shown by large standard deviations, likely reflecting differences in evaporation kinetics between samples. Such kinetic differences may arise from variations in crucible packing density and fill level, which alter the permeability of the powder bed and the diffusion rate of phosphate gas into the open atmosphere.

Decomposition of phase-pure OCP into the binary β-CPP/β-TCP assemblage releases six H_2O per formula unit (five from the hydrated layer and one from the condensation of two HPO_4 groups into P_2O_7), corresponding to a mass loss of 11.00 wt% in the absence of phosphate evaporation. Any loss of volatile phosphorous species adds to this baseline. For the two conditions repeated with gravimetric monitoring using pre-calcined crucibles, the measured mass losses were 11.32 ± 0.17 wt% (1000°C, 2 h, saturated) and 13.38 ± 0.13 wt% (1100°C, 24 h, open), in agreement with the values of 11.14 and 13.31 wt% calculated from the refined phase compositions of the same specimens by mass balance (Table 2). The gravimetric response to phosphate evaporation is small, however: between the mildest and the most extreme condition investigated, the total mass loss differs by only about 2 wt%, whereas the derived OCP_{eq} value differs by more than 40 wt%. The mass loss therefore serves as a consistency check but is not a sensitive measure of phosphate loss, and it is not used in the quantification procedure proposed here.

At 1100°C with atmosphere saturation, phosphate evaporation and compositional drift were reduced (ΔCaP = 0.012). However, fluctuations persisted, and large standard deviations at 8–24 h indicated reduced repeatability, again attributable to varying evaporation kinetics. Regression analysis still detected a small but significant downward drift (slope = –0.19 wt%/h, 95% CI [–0.37, –0.02], p = 0.034), indicating that atmosphere saturation reduces but does not fully eliminate phosphate loss at 1100°C.

At 1000°C without saturation, phosphate evaporation was negligible: Ca/P values varied by only ΔCaP = 0.0017, corresponding to an OCP_{eq} range of 1.0 wt%. OCP_{eq} values averaged 99.7 ± 0.5 wt% across

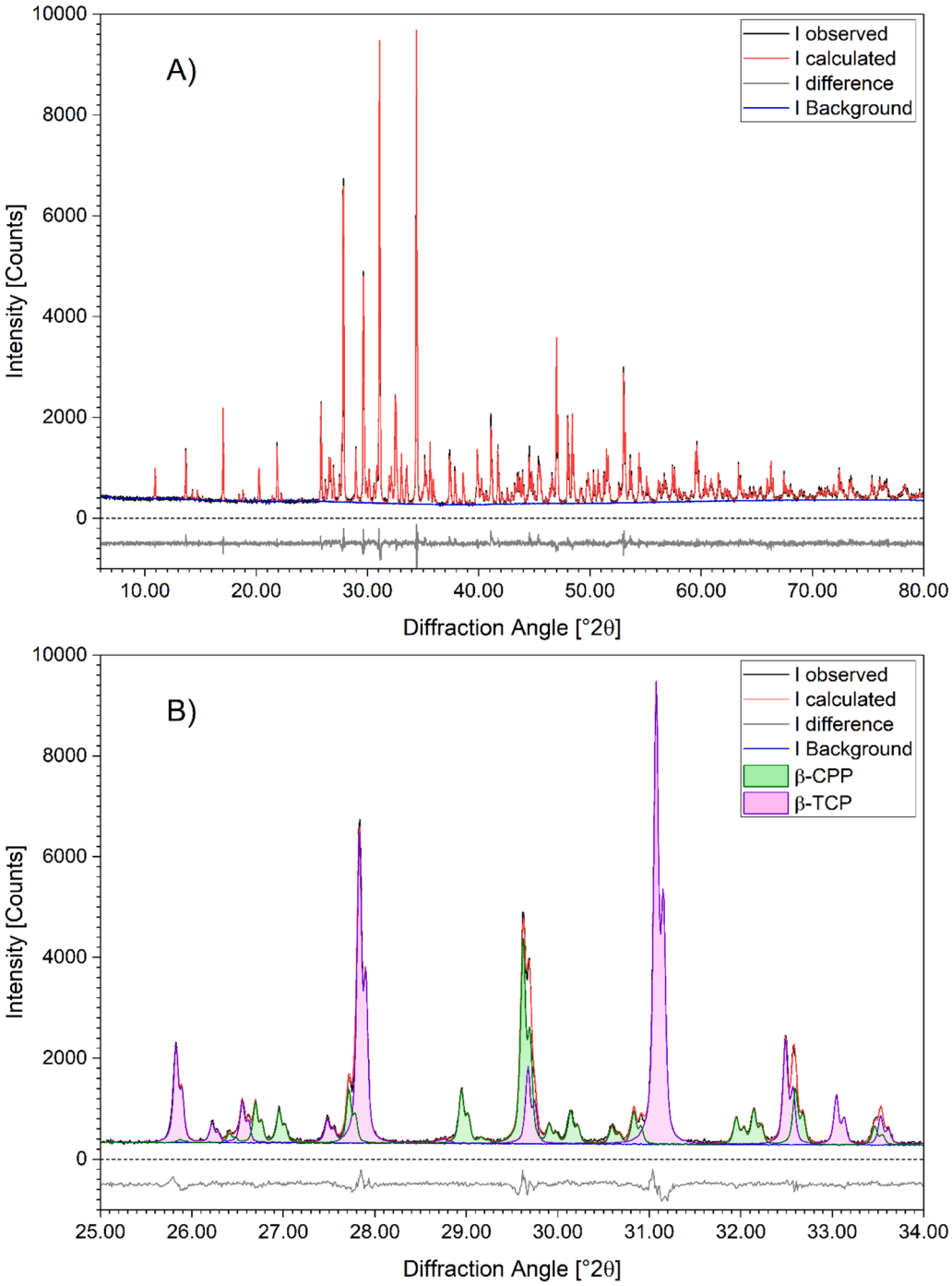

Fig. 3. A) shows a Rietveld refinement of a sample processed at 1100°C for 16 h in a phosphate-saturated atmosphere. The quality of fit is representative for all Rietveld refinements performed in this study. B) shows a detail view of the same dataset from 25.0 to 34.0° 2θ to demonstrate the separation of the β-CPP and β-TCP signals.

24 h. No significant drift was detected by linear regression (slope = +0.009 wt%/h, 95% CI [–0.027, +0.045], p = 0.59). Saturation further reduced variation (ΔCaP = 0.0013; OCP_{eq} range 0.7 wt%), yielding a mean of 100.3 ± 0.5 wt%. Values slightly above 100 wt% reflect minor artifacts from the Rietveld refinement. Linear regression confirmed the absence of drift (slope = +0.009 wt%/h, 95% CI [–0.029, +0.048], p = 0.62). At 1000°C, the OCP_{eq} value obtained after the shortest dwell time of 2 h (99.3 ± 0.3 wt% without and 100.0 ± 0.8 wt% with atmosphere saturation) was already indistinguishable from the value after 24 h. Conversion of the sample into the binary β-CPP/β-TCP assemblage was therefore complete within 2 h, and the observed plateau does not reflect incomplete recrystallization.

The pooled within-time-point standard deviation of OCP_{eq} was 0.58 wt% at 1000°C saturated and 0.46 wt% at 1000°C unsaturated, but increased to 2.07 wt% at 1100°C saturated and 3.97 wt% at 1100°C unsaturated. Levene's test confirmed that reproducibility differed significantly between the four conditions ($W = 3.98$, $p = 0.012$). A two-way ANOVA on OCP_{eq} pooled over dwell times revealed highly significant main effects of temperature ($F(1,56) = 58.4$, $p < 0.001$) and atmosphere ($F(1,56) = 37.0$, $p < 0.001$), and a strong temperature × atmosphere interaction ($F(1,56) = 33.8$, $p < 0.001$), indicating that atmosphere saturation had a substantially larger effect at

Table 1
Refined β-CPP contents, calculated Ca/P ratios, and equivalent OCP phase quantities (OCP_{eq}) for all calcination series at 1000°C and 1100°C, with and without atmosphere saturation. Values represent means ± standard deviations from triplicate measurements.

Temp. [°C] / Atmosphere	Time [h]	β-CPP [wt-%]	Ca/P [-]	OCP_{eq} [wt-%]
1100 / open	2	25.8 ± 0.2	1.3513 ± 0.0009	89.6 ± 0.6
	4	24.8 ± 0.2	1.3567 ± 0.0012	86.4 ± 0.7
	8	21.2 ± 2.4	1.3767 ± 0.0134	74.6 ± 7.9
	16	15.2 ± 1.1	1.4102 ± 0.0065	54.7 ± 3.9
	24	15.7 ± 0.3	1.4076 ± 0.0016	56.3 ± 0.9
	Mean	*20.5 ± 4.7*	*1.3805 ± 0.0262*	*72.3 ± 15.5*
1100 / saturated	2	28.2 ± 0.1	1.3379 ± 0.0003	97.3 ± 0.2
	4	29.0 ± 0.1	1.3339 ± 0.0007	99.7 ± 0.4
	8	28.3 ± 0.6	1.3374 ± 0.0034	97.6 ± 2.0
	16	26.7 ± 1.2	1.3459 ± 0.0064	92.7 ± 3.7
	24	27.6 ± 0.6	1.3410 ± 0.0031	95.5 ± 1.8
	Mean	*28.0 ± 0.9*	*1.3392 ± 0.0051*	*96.6 ± 3.0*
1000 / open	2	28.8 ± 0.1	1.3346 ± 0.0005	99.3 ± 0.3
	4	28.9 ± 0.1	1.3340 ± 0.0008	99.6 ± 0.4
	8	29.1 ± 0.1	1.3329 ± 0.0007	100.3 ± 0.4
	16	29.0 ± 0.0	1.3335 ± 0.0001	99.9 ± 0.1
	24	29.0 ± 0.3	1.3339 ± 0.0014	99.7 ± 0.8
	Mean	*29.0 ± 0.2*	*1.3338 ± 0.0009*	*99.7 ± 0.5*
1000 / saturated	2	29.0 ± 0.3	1.3334 ± 0.0014	100.0 ± 0.8
	4	29.1 ± 0.2	1.3330 ± 0.0009	100.2 ± 0.5
	8	29.3 ± 0.2	1.3321 ± 0.0009	100.7 ± 0.5
	16	29.2 ± 0.2	1.3328 ± 0.0011	100.3 ± 0.7
	24	29.2 ± 0.0	1.3327 ± 0.0002	100.3 ± 0.1
	Mean	*29.2 ± 0.2*	*1.3328 ± 0.0009*	*100.3 ± 0.5*

1100°C than at 1000°C. Tukey HSD post-hoc analysis showed that the 1100°C unsaturated condition differed significantly from each of the other three (all $p < 0.001$, mean differences in OCP_{eq} between 24.3 and 28.0 wt%), whereas the 1000°C saturated, 1000°C unsaturated, and 1100°C saturated conditions were statistically indistinguishable in mean OCP_{eq} (all $p > 0.5$). The latter three conditions thus yield comparable accuracy on average, but differ markedly in their dwell-time stability and their reproducibility across replicates.

4. Discussion

The calcination series confirmed that both temperature and dwell time strongly influence the stability of the β-CPP/β-TCP system. With prolonged dwell times, β-CPP gradually transforms into β-TCP as a result of the evaporation of volatile phosphorous species [17]. This alters the β-CPP/β-TCP ratio and drives the measured Ca/P ratio upward, thus biasing the estimation of OCP purity. Griesiute et al. [30] demonstrated that under more aggressive conditions (1200°C in vacuum), evaporation can lead to the complete transformation of β-CPP to β-TCP. Atmosphere saturation and minimization of free gas volume effectively reduced phosphate evaporation, though not completely at 1100°C. At 1000°C, evaporation was negligible even without saturation. Phosphate evaporation has been reported to depend strongly on furnace specifications, particularly the chamber volume and permeability [17]. In this study, the small furnace used (80 × 90 × 150 mm internal dimensions) showed no signs of evaporation at 1000°C, even without atmosphere saturation. However, this outcome cannot be generalized to larger or more permeable furnace chambers, where phosphate loss may occur even at 1000°C. The proposed atmosphere-saturation approach addresses this scalability concern directly: by placing the samples and the sacrificial monetite under an inverted crucible, the effective gas volume in equilibrium with the samples is reduced to a small, well-defined headspace, irrespective of the overall furnace dimensions. The saturation equilibrium between the sacrificial β-CPP and the gas phase is established locally within this headspace and is, to a first approximation, independent of furnace geometry, chamber permeability, or air exchange rate. Implementing atmosphere saturation is therefore strongly recommended for laboratories using furnaces of different sizes or designs, as it eliminates the need for furnace-specific calibration.

β-CPP and β-TCP are often described as being difficult to quantify from XRD data due to severe peak overlap among the two phases, and indeed three out of the four strongest β-CPP peaks ((2 0 2) at $d = 3.22169$ Å, (0 0 8) at $d = 3.01837$ Å, (1 0 8) at $d = 2.74865$ Å) overlap strongly with β-TCP peaks, thus compromising the quantification of small amounts of β-CPP in a β-TCP matrix. In a phase mixture representing a Ca/P ratio close to 1.3333, however, the β-CPP content is typically close to 29 wt-%, which is high enough to expose several additional peaks that are not affected by overlapping and allow for a reliable quantification (Fig. 3). The computational conversion of β-CPP and β-TCP quantities to equivalent OCP_{eq} values via calculation of the Ca/P ratio amplifies uncertainties by approximately 3.3-fold. Accurate results therefore require high-quality XRD data and a carefully validated refinement strategy. Following best practices for sample milling, preparation in the XRD sample holders, instrument alignment, data collection parameters, as well as for Rietveld refinement is therefore strongly recommended. The refinement should focus on accurate profile fitting taking into account all peak broadening effects and potential fine fractions from overmilling, as well as a realistic model for preferred orientation. The refinement strategy can be verified with a synthetic mixture of known composition (e.g., 29.06 wt% β-CPP + 70.94 wt% β-TCP, corresponding to $OCP_{eq} = 100.0$ wt%). This provides a benchmark to ensure accuracy and reproducibility of the method.

It should also be acknowledged that Rietveld refinement is an inherently model-dependent technique: a low goodness-of-fit indicator alone does not guarantee that all phases present have been correctly identified and quantified, particularly minor crystalline impurities or amorphous fractions whose contributions can be partially absorbed by the refined parameters of the included phases. Independent verification by a complementary technique, such as solid-state ^{31}P MAS NMR (Fig. 2) for the starting material, is therefore recommended whenever the absence of unaccounted phases needs to be established with high confidence.

In principle, the proposed framework for converting a bulk Ca/P ratio into an equivalent OCP content is independent of the analytical technique used to determine that ratio, and could in principle be combined with elemental methods such as ICP-MS, ICP-OES, or SEM-EDX. It should be noted, however, that the present method does not provide a direct measurement of the Ca/P ratio either: the high apparent precision (~0.001, absolute) results from error propagation of the refined β-CPP and β-TCP phase quantities (typical uncertainties of 0.1–0.3 wt%) through Eq. (3), which in the compositional range around Ca/P = 1.33 is comparatively insensitive to small variations in phase quantities. Even taking this into account, the precision of elemental alternatives is substantially lower in practice: reported relative standard deviations on Ca/P ratios are typically on the order of 0.5–5% for ICP-based methods [31] and 3–4% for SEM-EDX [32]. Because the conversion of Ca/P to OCP_{eq} amplifies uncertainties by approximately 3.3-fold, elemental Ca/P determinations would translate into OCP_{eq} uncertainties in the order of several to several tens of wt%, severely limiting their usefulness for phase purity assessment.

The indirect quantification method for OCP phase purity presented here is relatively simple to implement and only requires a high-temperature furnace and XRD equipment with Rietveld refinement. The OCP phase content is then derived from the bulk Ca/P ratio calculated from the refined high-temperature phase composition. However, the procedure relies on two assumptions: (i) that OCP and CDHA (and/or ACP) are the only phases present in the starting material, and (ii) that their Ca/P ratios are fixed at 1.33 and 1.50, respectively. Preliminary XRD analysis of the raw samples is therefore essential to exclude additional phases. If revised values for endmember Ca/P ratios emerge in literature, or if additional phases are detected in the raw samples, the calculation procedure needs to be adapted accordingly.

The present validation was carried out on a phase-pure OCP batch,

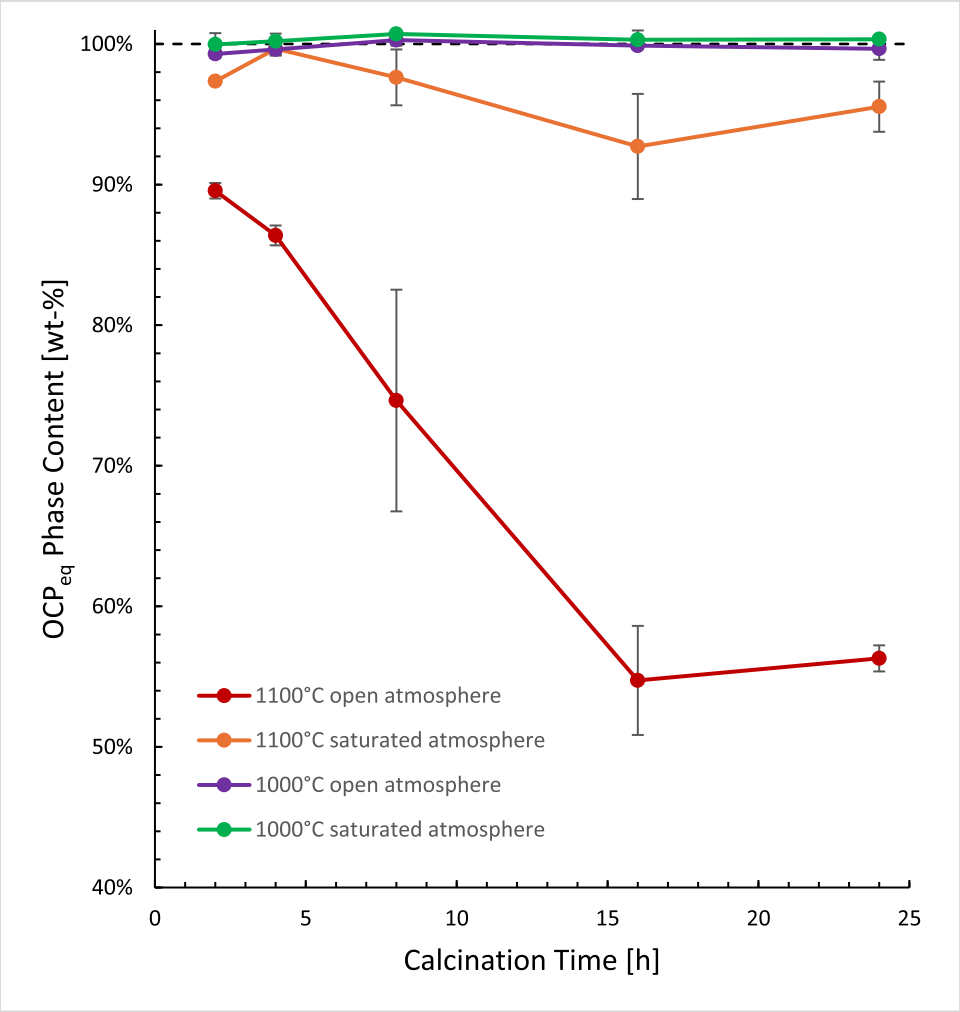

Fig. 4. Calculated OCP_{eq} phase content for all calcination series at 1000 and 1100°C, without ("open") and with ("saturated") atmosphere saturation.

Table 2
Measured and calculated mass loss (Δm) for two calcination conditions repeated with gravimetric monitoring. Calculated values were obtained from the refined β-TCP and β-CPP contents of the same specimens by mass balance, taking phase-pure OCP as the starting composition and calcium as the conserved component. Values are single determinations; uncertainties on the phase quantities are estimated standard deviations of the Rietveld refinement, those on the measured mass loss are propagated from the weighings.

Condition	β-TCP [wt %]	β-CPP [wt %]	Δm calculated [wt%]	Δm measured [wt%]
Phase-pure OCP, no phosphate loss (theoretical)	70.94	29.06	11.00	–
1000°C, 2 h, saturated	71.77 ± 0.14	28.23 ± 0.14	11.14	11.32 ± 0.17
1100°C, 24 h, open	84.49 ± 0.13	15.51 ± 0.13	13.31	13.38 ± 0.13

which establishes the robustness and repeatability of the method under varying thermal treatment conditions. Confirming the assumed end-member Ca/P ratios on partially hydrolyzed samples of independently determined composition would further extend its scope to mixtures with high CDHA contents.

5. Conclusions

Direct quantification of OCP and CDHA by XRD is unreliable due to severe peak overlap. Determining the molar Ca/P ratio after controlled calcination provides a simple and effective indirect approach to assess OCP phase purity. However, suppressing phosphate evaporation is critical to preserve the original Ca/P ratio, and we demonstrate a practical method using sacrificial monetite to saturate the atmosphere with phosphorus species. Stable and reproducible OCP phase purity values were obtained throughout the entire dwell-time range from 2 to 24 h at 1000°C in saturated atmosphere, with conversion into the binary β-CPP/β-TCP assemblage already complete after the shortest dwell time investigated. We therefore recommend a calcination at 1000°C for 2 h in a phosphate-saturated atmosphere as the standard protocol. This is a substantial reduction relative to the 15 h specified in ISO 13779–3, and is justified by the demonstrated insensitivity of the result to dwell time. Atmosphere saturation is recommended irrespective of dwell time, since it renders the result independent of furnace geometry and permeability. The approach is straightforward, reproducible, and adaptable, offering a robust tool for both research applications and quality control of OCP-based biomaterials.

Declaration of generative AI and AI-assisted technologies in the manuscript preparation process

During the preparation of this work, the authors used Claude Opus 5

(Anthropic), accessed via claude.ai, in order to improve the structure and language of the manuscript and to obtain guidance on the statistical evaluation, which was performed by the authors using Origin 2026 (OriginLab). After using this tool, the authors reviewed and edited the content as needed and take full responsibility for the content of the published article.

CRediT authorship contribution statement

Nicola Döbelin: Writing – original draft, Visualization, Software, Methodology, Investigation, Formal analysis, Data curation, Conceptualization. **Ryo Hamai:** Writing – review & editing, Resources, Methodology, Investigation. **Kaori Tsuchiya:** Writing – review & editing, Resources, Methodology, Investigation. **Osamu Suzuki:** Writing – original draft, Supervision, Resources, Project administration, Methodology, Funding acquisition, Formal analysis, Data curation, Conceptualization.

Declaration of competing interest

The authors declare the following financial interests/personal relationships which may be considered as potential competing interests: Osamu Suzuki reports financial support was provided by Japan Society for the Promotion of Science. Osamu Suzuki has patent #JP 6786227 B2 issued to Tohoku University and Japan Fine Ceramics Co., Ltd. All other authors declare that they have no known competing financial interests or personal relationships that could have appeared to influence the work reported in this paper.

Acknowledgements

Funding: This work was supported by MEXT/JSPS KAKENHI under grant numbers JP21K19586, JP21H03121, and JP24K02624.

Data availability

https://doi.org/10.5281/zenodo.18326854

References

[1] W.E. Brown, Crystal growth of bone mineral, Clin. Orthop. 44 (1966) 205–220.
[2] W.E. Brown, J.P. Smith, J.R. Lehr, A.W. Frazier, Crystallographic and chemical relations between octocalcium phosphate and hydroxyapatite, Nature 196 (1962) 1050–1055, https://doi.org/10.1038/1961050a0.
[3] P. Simon, D. Grüner, H. Worch, W. Pompe, H. Lichte, T. El Khassawna, C. Heiss, S. Wenisch, R. Kniep, First evidence of octacalcium phosphate@osteocalcin nanocomplex as skeletal bone component directing collagen triple–helix nanofibril mineralization, Sci. Rep. 8 (2018) 13696, https://doi.org/10.1038/s41598-018-31983-5.
[4] I. Kovrlija, J. Locs, D. Loca, Octacalcium phosphate: innovative vehicle for the local biologically active substance delivery in bone regeneration, Acta Biomater. 135 (2021) 27–47, https://doi.org/10.1016/j.actbio.2021.08.021.
[5] O. Suzuki, Octacalcium phosphate: osteoconductivity and crystal chemistry, Acta Biomater. 6 (2010) 3379–3387, https://doi.org/10.1016/j.actbio.2010.04.002.
[6] O. Suzuki, R. Hamai, S. Sakai, The material design of octacalcium phosphate bone substitute: increased dissolution and osteogenecity, Acta Biomater. 158 (2023) 1–11, https://doi.org/10.1016/j.actbio.2022.12.046.
[7] O. Suzuki, G. Insley (Eds.), Octacalcium Phosphate Biomaterials: Understanding of Bioactive Properties and Application, Woodhead Publishing, Cambridge, MA, 2020.
[8] M. Mathew, W.E. Brown, L.W. Schroeder, B. Dickens, Crystal structure of octacalcium bis(hydrogenphosphate) tetrakis(phosphate)pentahydrate, $Ca_8(HPO_4)_2(PO_4)_4\times5H_2O$, J. Crystallogr. Spectrosc. Res. 18 (1988) 235–250, https://doi.org/10.1007/BF01194315.
[9] B.B. Tomazic, M.S. Tung, T.M. Gregory, W.E. Brown, Mechanism of hydrolysis of octacalcium phosphate, Scanning Microsc. 3 (1989) 119–127.
[10] Y.H. Tseng, C.Y. Mou, J.C.C. Chan, Solid-state NMR study of the transformation of octacalcium phosphate to hydroxyapatite: a mechanistic model for central dark line formation, J. Am. Chem. Soc. 128 (2006) 6909–6918, https://doi.org/10.1021/ja060336u.
[11] E.D. Eanes, Thermochemical studies on amorphous calcium phosphate, Calcif. Tissue Res. 5 (1970) 133–145, https://doi.org/10.1007/bf02017543.
[12] W.J.E.M. Habraken, J. Tao, L.J. Brylka, H. Friedrich, L. Bertinetti, A.S. Schenk, A. Verch, V. Dmitrovic, P.H.H. Bomans, P.M. Frederik, J. Laven, P. Van Der Schoot, B. Aichmayer, G. De With, J.J. DeYoreo, N.A.J.M. Sommerdijk, Ion-association complexes unite classical and non-classical theories for the biomimetic nucleation of calcium phosphate, Nat. Commun. 4 (2013), https://doi.org/10.1038/ncomms2490. Article number 1507.
[13] K. Sudarsanan, R.A. Young, Significant precision in crystal structural details: holly springs hydroxyapatite, Acta Crystallogr. B 25 (1969) 1534–1543, https://doi.org/10.1107/S0567740869004298.
[14] D.G.A. Nelson, J.D. McLean, High-resolution electron microscopy of octacalcium phosphate and its hydrolysis products, Calcif. Tissue Int. 36 (1984) 219–232, https://doi.org/10.1007/BF02405321.
[15] D.G.A. Nelson, H. Salimi, G.H. Nancollas, Octacalcium phosphate and apatite overgrowths: a crystallographic and kinetic study, J. Colloid Interface Sci. 110 (1986) 32–39, https://doi.org/10.1016/0021-9797(86)90350-4.
[16] O. Suzuki, H. Yagishita, M. Yamazaki, T. Aoba, Adsorption of bovine serum albumin onto octacalcium phosphate and its hydrolyzates, Cells Mater. 5 (1995) 45–54.
[17] N. Döbelin, Y. Maazouz, R. Heuberger, M. Bohner, A.A. Armstrong, A.J. Wagoner Johnson, C. Wanner, A thermodynamic approach to surface modification of calcium phosphate implants by phosphate evaporation and condensation, J. Eur. Ceram. Soc. 40 (2020) 6095–6106, https://doi.org/10.1016/j.jeurceramsoc.2020.07.028.
[18] O. Suzuki, M. Nakamura, Y. Miyasaka, M. Kagayama, M. Sakurai, Bone-formation on synthetic precursors of hydroxyapatite, Tohoku J. Exp. Med. 164 (1991) 37–50, https://doi.org/10.1620/tjem.164.37.
[19] Y. Honda, S. Kamakura, K. Sasaki, O. Suzuki, Formation of bone-like apatite enhanced by hydrolysis of octacalcium phosphate crystals deposited in collagen matrix, J. Biomed. Mater. Res. B Appl. Biomater. 80B (2007) 281–289, https://doi.org/10.1002/jbm.b.30595.
[20] International Organization for Standardization (ISO). 13779-3: Implants for Surgery–Hydroxyapatite–Part 3: Chemical Analysis and Characterization of Crystallinity and Phase Purity Second Ed., 2018, ISO Standard, 2018.
[21] W. Sauskojus, J.K. Wied, C.F. Litterscheid, M. Mangstl, J. Schmedt Auf Der Günne, Crystal structure of γ-$Ca_2P_2O_7$, Z. Anorg. Allg. Chem. 648 (2022), https://doi.org/10.1002/zaac.202200196.
[22] N. Doebelin, R. Kleeberg, Profex: a graphical user interface for the Rietveld refinement program BGMN, J. Appl. Crystallogr. 48 (2015) 1573–1580, https://doi.org/10.1107/S1600576715014685.
[23] B. Dickens, L.W. Schroeder, W.E. Brown, Crystallographic studies on the role of Mg as a stabilizing impurity in β-$Ca_3(PO_4)_2$ I. The crystal structure of pure β-$Ca_3(PO_4)_2$, J. Solid State Chem. 10 (1974) 232–248, https://doi.org/10.1016/0022-4596(74)90030-9.
[24] S. Boudin, A. Grandin, M.M. Borel, A. Leclaire, B. Raveau, Redetermination of the β-$Ca_2P_2O_7$ structure, Acta Crystallogr. C 49 (1993) 2062–2064, https://doi.org/10.1107/S0108270193005608.
[25] B.O. Fowler, M. Markovic, W.E. Brown, Octacalcium phosphate. 3. Infrared and Raman vibrational spectra, Chem. Mater. 5 (1993) 1417–1423, https://doi.org/10.1021/cm00034a009.
[26] Y.H. Tseng, J. Zhan, K.S.K. Lin, C.Y. Mou, J.C.C. Chan, High resolution ^{31}P NMR study of octacalcium phosphate, Solid State Nucl. Magn. Reson. 26 (2004) 99–104, https://doi.org/10.1016/j.ssnmr.2004.06.002.
[27] E. Davies, M.J. Duer, S.E. Ashbrook, J.M. Griffin, Applications of NMR crystallography to problems in biomineralization: refinement of the crystal structure and ^{31}P solid-state NMR spectral assignment of octacalcium phosphate, J. Am. Chem. Soc. 134 (2012) 12508–12515, https://doi.org/10.1021/ja3017544.
[28] C. Jäger, T. Welzel, W. Meyer Zaika, M. Epple, A solid state NMR investigation of the structure of nano crystalline hydroxyapatite, Magn. Reson. Chem. 44 (2006) 573–580, https://doi.org/10.1002/mrc.1774.
[29] A.P. Legrand, H. Sfihi, N. Lequeux, J. Lemaître, ^{31}P solid-state NMR study of the chemical setting process of a dual-paste injectable brushite cements, J. Biomed. Mater. Res. Part B Appl. Biomater. 91 (2009) 46–54, https://doi.org/10.1002/jbm.b.31372.
[30] D. Griesiute, E. Raudonyte-Svirbutaviciene, A. Kareiva, A. Zarkov, The influence of annealing conditions on the Ca/P ratio and phase transformations in bulk calcium phosphates, CrystEngComm 24 (2022) 1166–1170, https://doi.org/10.1039/d1ce01625c.
[31] A. Szymczycha-Madeja, M. Welna, M. Zabłocka-Malicka, P. Pohl, W. Szczepaniak, Development and validation of an analytical method for determination of Al, Ca, Cd, Fe, Mg and P in calcium-rich materials by ICP OES, Molecules 26 (2021) 6269, https://doi.org/10.3390/molecules26206269.
[32] F. Miculescu, C. Luță, A.E. Constantinescu, A. Maidaniuc, A.C. Mocanu, M. Miculescu, Ş.I. Voicu, L.T. Ciocan, Considerations and influencing parameters in EDS microanalysis of biogenic hydroxyapatite, J. Funct. Biomater. 11 (2020) 82, https://doi.org/10.3390/jfb11040082.